

Integrated dual-band multiple-input multiple-output antenna module using higher mode control for 5G applications

Longyue Qu¹  | Haiyan Piao²

¹School of Electronics and Information Engineering, Harbin Institute of Technology, Shenzhen, China

²Research and Development Department, Hanyang Antenna Design Co. Ltd, Shenzhen, China

Correspondence

Longyue Qu, School of Electronics and Information Engineering, Harbin Institute of Technology, Shenzhen, China.
Email: rioinkorea@gmail.com

Abstract

This study presents a self-decoupled and highly integrated multiple-input multiple-output (MIMO) antenna pair for the 3.5 GHz (3.4–3.6 GHz) and 5 GHz (4.8–5 GHz) frequency bands, where a loop-type antenna and a dipole-type antenna are assembled into the front and backside of a compact modular board. A tuning inductor and a tuning capacitor are employed in the loop-type antenna and the dipole-type antenna, respectively, for higher mode resonance control, such that the dominant mode and higher mode of each antenna element are excited to achieve dual-band operation. Herein, the dominant modes of the loop-type antenna and the dipole-type antenna are orthogonal to each other, contributing to the self-decoupling effect in the lower band. Otherwise, the modal orthogonality of the higher modes of the two antennas is responsible for the high-isolated performance of the higher band. In this way, the proposed dual-band MIMO antenna module obtains a high spatial utilization ratio, even though they are disposed of in the same volume. The MIMO antenna module can produce impedance bandwidths above 200 MHz at both frequency bands, and the isolation within the lower and higher bands is above 16.5 and 13.5 dB, respectively. Additionally, an 8×8 MIMO antenna array is further constructed and measured. In measurement, the total efficiencies are higher than 60%, and the envelope correlation coefficient values are all below 0.1. Therefore, it is demonstrated that the proposed technique can be promisingly applied in large-scale MIMO antenna systems for current and future terminal devices, having advantages in multiband operation, high integration, and inherent isolation.

KEYWORDS

inherence isolation, MIMO, modal orthogonality, modular board, multiband operation

1 | INTRODUCTION

The next-generation communication (5G) is now drawing much attention due to an avalanche of wireless traffic from increasing user numbers and more powerful

cellular devices demanding high-quality, low latency video, and multimedia applications. This tremendous demand for mobile data rates brings extraordinary challenges for wireless service providers to overcome a global bandwidth shortage since the current frequency

spectrum is intensively limited to the range below 3 GHz. For this reason, the sub-6 GHz band is deployed to address a compromise between capacity and coverage.^{1,2} Meanwhile, large-scale multiple-input multiple-output (MIMO) antenna elements are required in both base stations and terminal devices to achieve ultra-fast speeds, low latency, and excellent reliability.³

Nevertheless, large-scale MIMO antennas with high isolation and low correlation have always been challenging issues, especially in crowded terminal devices where compactness must be addressed. In the literature, various solutions have been presented, offering important features such as large scale and integration.^{4–12} Although large-scale antenna elements can be possibly allocated to the volume-constraint terminals, the required antenna distance is still large, and the integration level is not high enough. More importantly, most of the aforementioned techniques are only in narrow-band or single-band operation.

Herein, candidate solutions to wideband and multi-band MIMO antennas for 5G applications were studied in References 13–30. However, vast distances and large footprints are required in^{13–16} because the antenna elements are spatially distributed in the system ground plane. Various decoupling structures^{17–21} and neutralization lines or components^{22–26} are introduced to enhance the isolation performance and reduce the distance between antenna elements. The main drawback of these solutions is their complicated tuning process, low integration level, and large-sized implementation volume. In References 27–30, self-decoupled MIMO antennas based on pattern diversity and modal orthogonality are proposed, in which way, close antenna distance, and high integration level are obtained. However, difficult matching networks are required in References 27,28, and both the upper and lower sides of the system ground plane are inevitably occupied in References 29,30, which may be undesired in practical scenarios.

To circumvent the abovementioned disadvantages, a dual-band MIMO module is presented in a simple and straightforward method, free of decoupling structures, complicated matching components, or specific construction processes. In this study, a loop-type antenna and a dipole-type antenna are printed on the front side and backside of a modular board. Meanwhile, the dominant mode and the higher mode of each antenna element are simultaneously excited to operate at the 3.5 GHz (3.4–3.6 GHz) and 5 GHz (4.8–5 GHz) bands, respectively. In Reference 31, a similar dipole-type antenna was used to form a MIMO antenna pair, but only a single band was obtained, and its integration level is not high. Accordingly, the main contribution of this study is that a dual-band dual-antenna pair is successfully integrated into a

modular board by merely utilizing lumped elements. Particularly, in the low band, the half-wavelength dipole mode and the half-wavelength loop mode are self-isolated; in the high band, the one-wavelength dipole mode and the one-wavelength loop mode also have polarization orthogonality. This particular feature of the proposed technique is reported as the first of its kind.

The rest of this manuscript is organized as follows. In Section 2, the proposed dual-band MIMO antenna module is described, and its operation mechanism is explained. In Section 3, the fabrication of an 8×8 MIMO antenna array was conducted to demonstrate the practicality of the proposed technique for 5G applications.

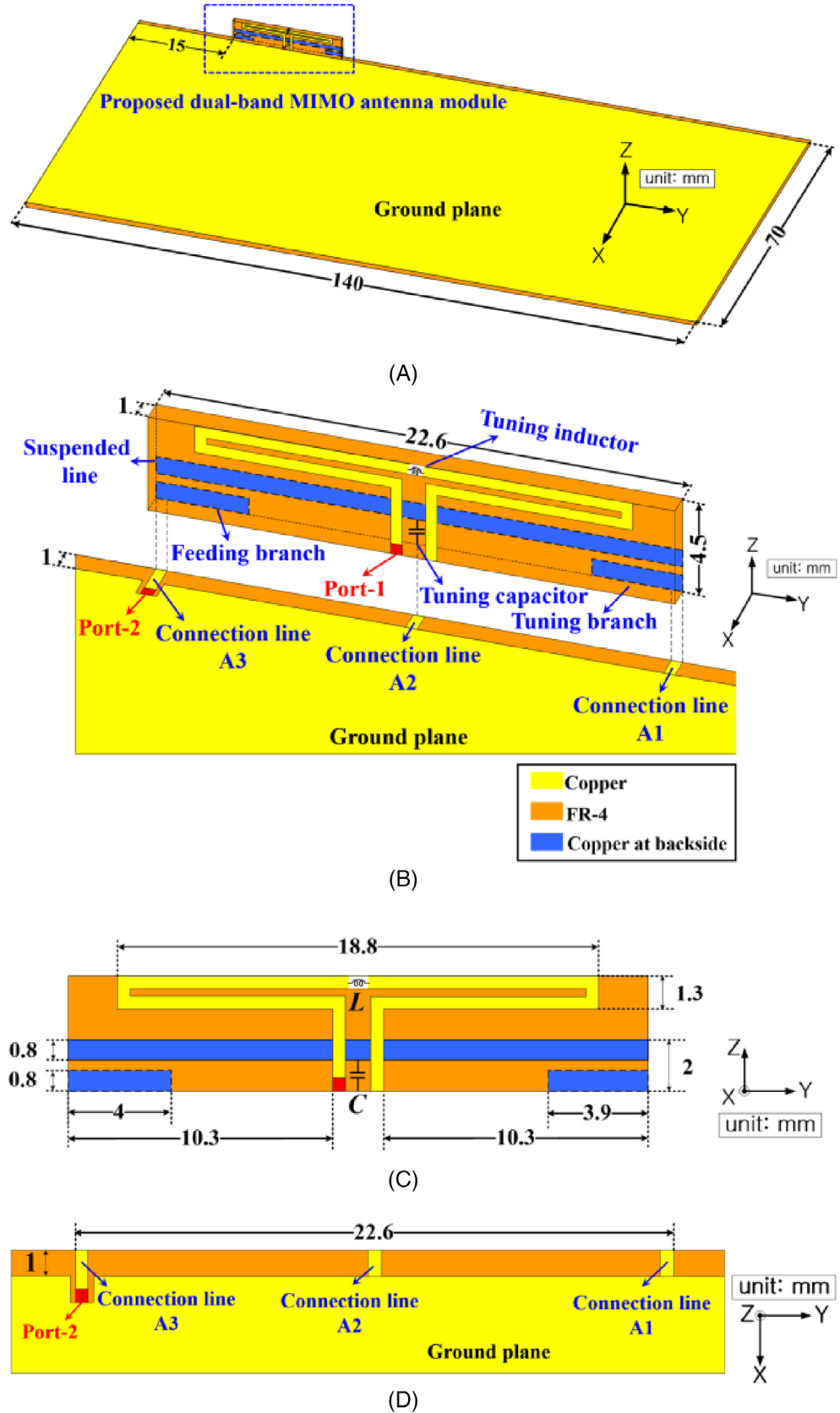
2 | DUAL-BAND MIMO ANTENNA MODULE

2.1 | Antenna configuration

Figure 1 depicts the configurations of the proposed dual-band MIMO antenna module, where a loop-type antenna (Antenna-1) and a dipole-type antenna (Antenna-2) are printed on the front side and backside of the module, respectively. Different from the antenna designs in the literature, the proposed modular board includes two independent antenna elements overlapping each other, such that high integration level is accomplished. The module has a dimension of $4.5 \text{ mm} \times 22.6 \text{ mm} \times 1 \text{ mm}$ and is vertically installed along the edge of a $70 \text{ mm} \times 140 \text{ mm}$ ground plane. The FR4 substrate ($\epsilon_r = 4.4$, $\tan \delta = 0.02$) with a thickness of 1 mm is used to model the modular board and the ground plane. Meanwhile, 1-mm ground clearance is reserved at the edge side of the ground plane for the simple installation of the modules, so the overall dimension of the substrate is $71 \text{ mm} \times 140 \text{ mm}$. It is noted that the dimension of the platform is chosen as a case study of a popularly used smartphone. Detailed information on the proposed dual-band MIMO antenna module can be found by referring to Figure 1B–D.

In Figure 1, the loop-type antenna is symmetrically printed at the front side of the module (yellow solid trace), which is directly fed by a voltage source at one end and shorted to the ground plane at the other end. A tuning inductor (L) is loaded at the center of the upper trace of the loop-type antenna for higher mode control without affecting the dominant mode. In this way, dual-band operation can be obtained by merely utilizing a single loop structure. The loop-type antenna has a folded structure to adjust the input impedance so that good impedance matching can be simultaneously obtained at both operation bands. It is noted that the

FIGURE 1 Configurations of the proposed dual-band multiple-input multiple-output antenna module: (A) perspective view, (B) implementation of the modular board, (C) zoomed view of the modular board, and (D) zoomed view of the ground plane



overall dimension of the loop-type antenna is 4.5 mm × 18.8 mm, and the optimized value of L is 2.5 nH. Besides, the width of the conductor traces is set as 0.5 mm.

The dipole-type antenna is printed at the backside of the modular board (blue dash trace), overlapping partly with the loop-type antenna. It consists of a suspended line, a tuning branch, a tuning capacitor C , and a feeding

branch. The suspended line is dominantly responsible for radiation, whose dominant mode and higher mode can be easily controlled by the tuning branch at the right edge and the tuning capacitor at the center, respectively. A connection line A1, printed on the ground clearance, is used to connect the tuning branch and the ground plane so that the tuning branch operates as a capacitive load to the suspended line, responsible for resonance control without modifying the dimension of the suspended line. A connection line A2 is also printed on the ground clearance so that the tuning capacitor C is loaded between the ground plane and the center of the suspended line to selectively control the higher mode resonance. Moreover, the feeding branch is connected to the CPW line through the connection line A3 so that the RF signal from a voltage source is fed into the feeding branch. In this way, the feeding branch capacitively excites the suspended line and controls the antenna's input impedance. It is noted that the dipole-type antenna occupies an overall dimension of $2 \text{ mm} \times 22.6 \text{ mm}$, and the optimized capacitor value of C is 0.4 pF .

2.2 | Simulation results and operation mechanism

The simulated scattering parameters (S -parameters) of the proposed MIMO antenna module are presented in Figure 2, where dual-band operation can be observed. At the 3.5 GHz band, the 3:1 VSWR bandwidths for Antenna-1 and Antenna-2 are 440 MHz (from 3.28 to 3.72 GHz) and 280 MHz (from 3.35 to 3.63 GHz), respectively; the bandwidths at the 5 GHz band are 530 MHz (from 4.61 to 5.14 GHz) and 390 MHz (from 4.72 to 5.11 GHz). As observed in the S_{12} curve, the isolation

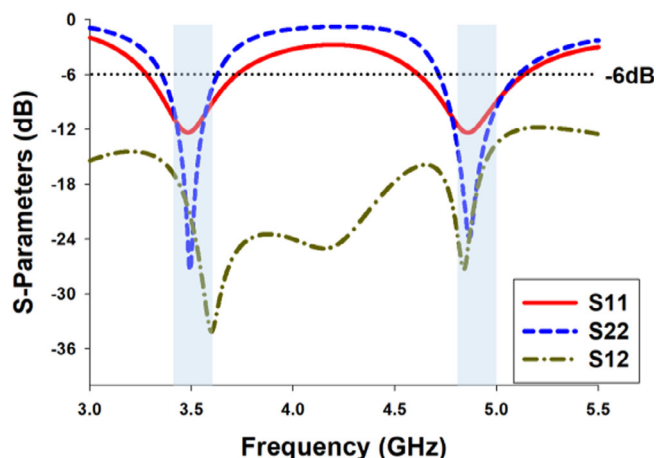


FIGURE 2 Simulated S -parameters of the proposed dual-band multiple-input multiple-output antennas

within the lower and higher frequency bands are above 16.5 and 13.5 dB , respectively, indicating that the proposed MIMO antenna pair can achieve self-decoupled performance in both operation bands.

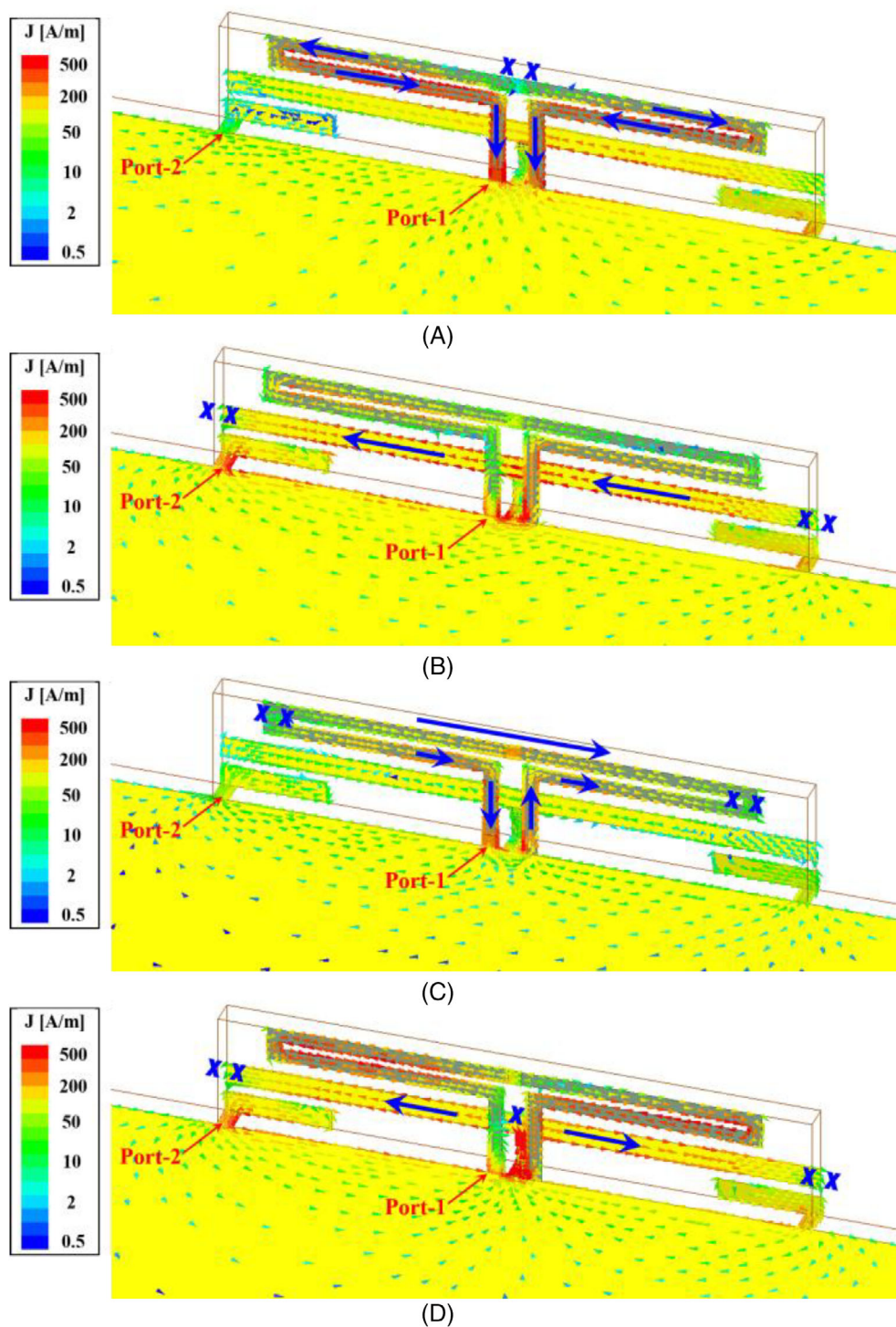
To further understand the operation mechanism of the proposed technique, simulated surface current distributions at 3.5 and 5 GHz are plotted in Figure 3. It is noted that the simulated current distributions are obtained when one port is excited while the other is 50Ω terminated.

The current distributions at 3.5 GHz of the loop-type antenna (Port-1) and the dipole-type antenna (Port-2) are illustrated in Figure 3A,B, respectively. In Figure 3A, the loop-type antenna has current nulls at the center of the upper trace, which resembles a half-wavelength resonance (the dominant mode of the loop-type antenna). As can be observed from Figure 3B, the dipole-type antenna produces in-phase current flows along the suspended line, which resembles a half-wavelength resonance (the dominant mode of the dipole-type antenna). In the 3.5 GHz band, accordingly, the current modes of both antenna elements are intrinsically orthogonal, and this feature determines the fact that extremely weak currents are induced from one port to another.

The current distributions at 5 GHz of the loop-type antenna (Port-1) and the dipole-type antenna (Port-2) are shown in Figure 3C,D, respectively. In Figure 3C, it can be seen that the loop-type antenna generates two current nulls, indicating the one-wavelength mode resonance (the higher mode of the loop-type antenna) is operating. For the loop-type antenna, it is worthy to note that the tuning inductor L is located at the current maximum positions of the higher mode and the current nulls positions of the dominant mode, thereby selectively controlling the one-wavelength resonance without affecting the half-wavelength resonance. In Figure 3D, it is apparent that the dipole-type antenna produces current nulls at the center of the suspended line, resembling a one-wavelength resonance (the higher mode of the dipole-type antenna). For the dipole-type antenna, since the tuning capacitor C is located at the current maximum positions of the dominant mode and the current null positions of the higher mode, the tuning capacitor C selectively controls the one-wavelength resonance without affecting its half-wavelength resonance. Accordingly, the higher modes of the two antenna elements also have modal orthogonality, which determines their high isolation property in the higher band.

Schematic structures are demonstrated in Figure 4 for a better understanding of the construction process of the proposed dual-band MIMO antenna module. Figure 4A presents the integration process of the MIMO antenna pair at the lower band. The dominant mode of the loop-

FIGURE 3 Simulated surface current distributions: (A) Port 1 excited at 3.5 GHz, (B) Port 2 excited at 3.5 GHz, (C) Port 1 excited at 5 GHz, and (D) Port 2 excited at 5 GHz



type antenna in Design I and the dominant mode of the dipole-type antenna in Design II are orthogonal to each other and can be assembled as Design III, where the two antenna elements are placed at the upper and lower sides of the ground plane. Though a similar implementation method utilizing a dipole-type antenna and a T-monopole antenna was presented in,³¹ a combination of a loop-type antenna³² and a dipole-type antenna³¹ has not been reported in the literature. Finally, Design III is further

transformed into Design IV, exploiting only one side of the ground plane and reusing the space of the modular board. In this way, a higher integration level than^{29–31} is accomplished.

Similarly, Figure 4B demonstrates the integration process of the MIMO antenna pair at the higher band. The higher mode of the loop-type antenna in Design I and the higher mode of the dipole-type antenna in Design II, having modal orthogonality, can be integrated as shown in

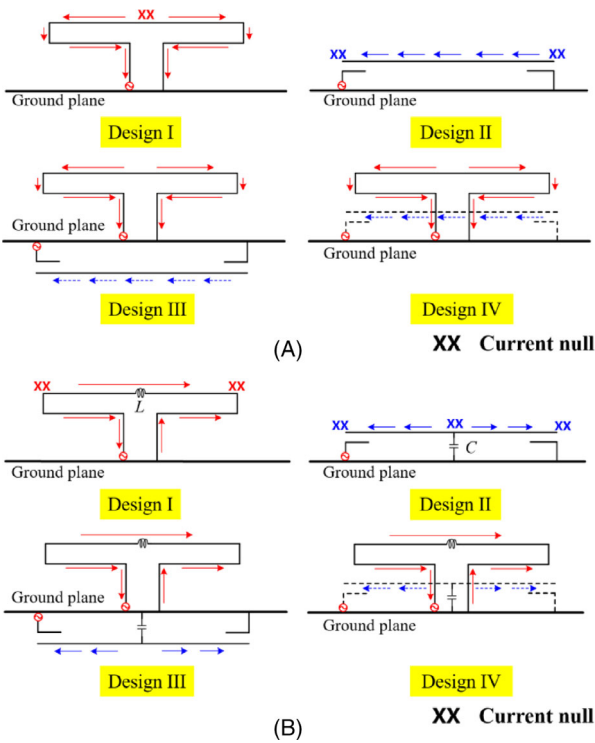


FIGURE 4 Schematic of the proposed self-decoupled dual-band multiple-input multiple-output antenna pair: (A) at the lower band and (B) at the higher band

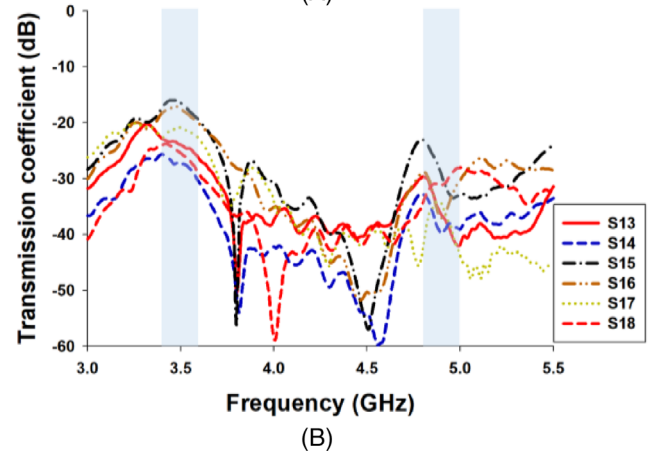
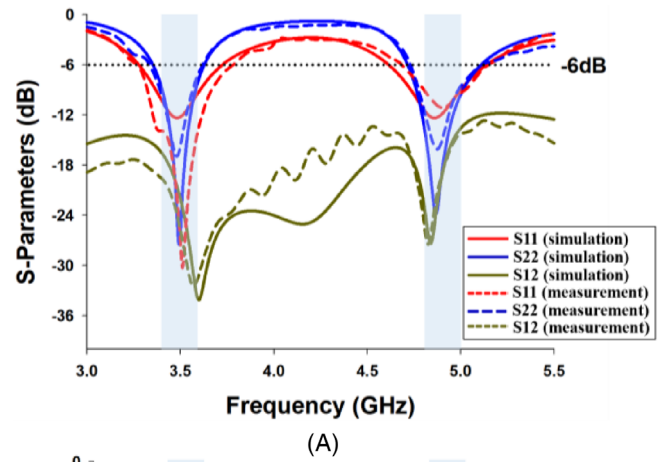


FIGURE 6 Measured S-parameters: (A) S-parameters and (B) transmission coefficients

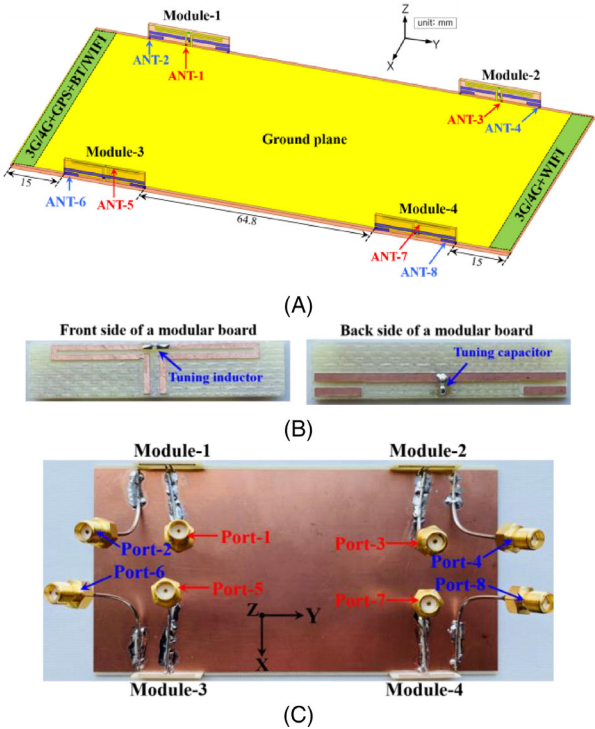


FIGURE 5 8 × 8 multiple-input multiple-output antenna array: (A) simulation model, (B) fabricated modular board before assembly, and (C) fabrication after assembly

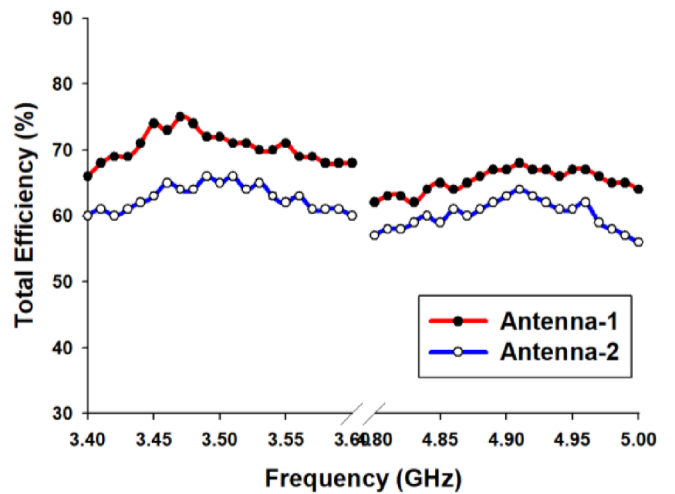


FIGURE 7 Measured total radiation efficiencies

Design III. Design IV achieves a higher spatial utilization ratio by fully exploiting the front and backside of the modular board. Accordingly, a self-decoupled dual-band MIMO antenna module, having a high integration level and spatial utilization ratio, can be obtained by utilizing modal orthogonality and higher mode control.

According to the aforementioned description, the orthogonality in both the dominant mode and the higher mode is the critical factor to guarantee dual-band operation and high isolation properties. Meanwhile, it is important to design symmetrical structures to accessibly realize current symmetry and modal orthogonality. Besides, there are many other feasible alternatives to the proposed technique. For example, the loop-type antenna is popularly adopted because of its freedom in structural implementation and impedance adjustment.³² Therefore, the loop-type antenna can be designed in different structures and have varied impedances, in which case, the tuning inductor L should be varied for the control of the higher mode resonance. Following the procedure in Figure 4, dual-band operation and high isolation can be easily accessed. It is worthy to note that the feeding methods are the least factors that should be considered in antenna design because the orthogonality in the

antenna structures is merely affected by the feeding methods when exciting the antenna elements.

3 | DEMONSTRATION OF 8 × 8 MIMO ANTENNA ARRAY

3.1 | Antenna array configuration

In this section, a large-scale MIMO antenna array is demonstrated by duplicating the aforementioned antenna module, intended for current and future 5G terminal devices. For this purpose, an 8 × 8 MIMO antenna system is established in Figure 5 as a case study, where four modular boards are allocated along the long sides of the ground plane. Detailed information can be found by referring to Figure 5A. Moreover, the fabricated prototypes of the assembled fabrication are pictured in Figure 5B,C.

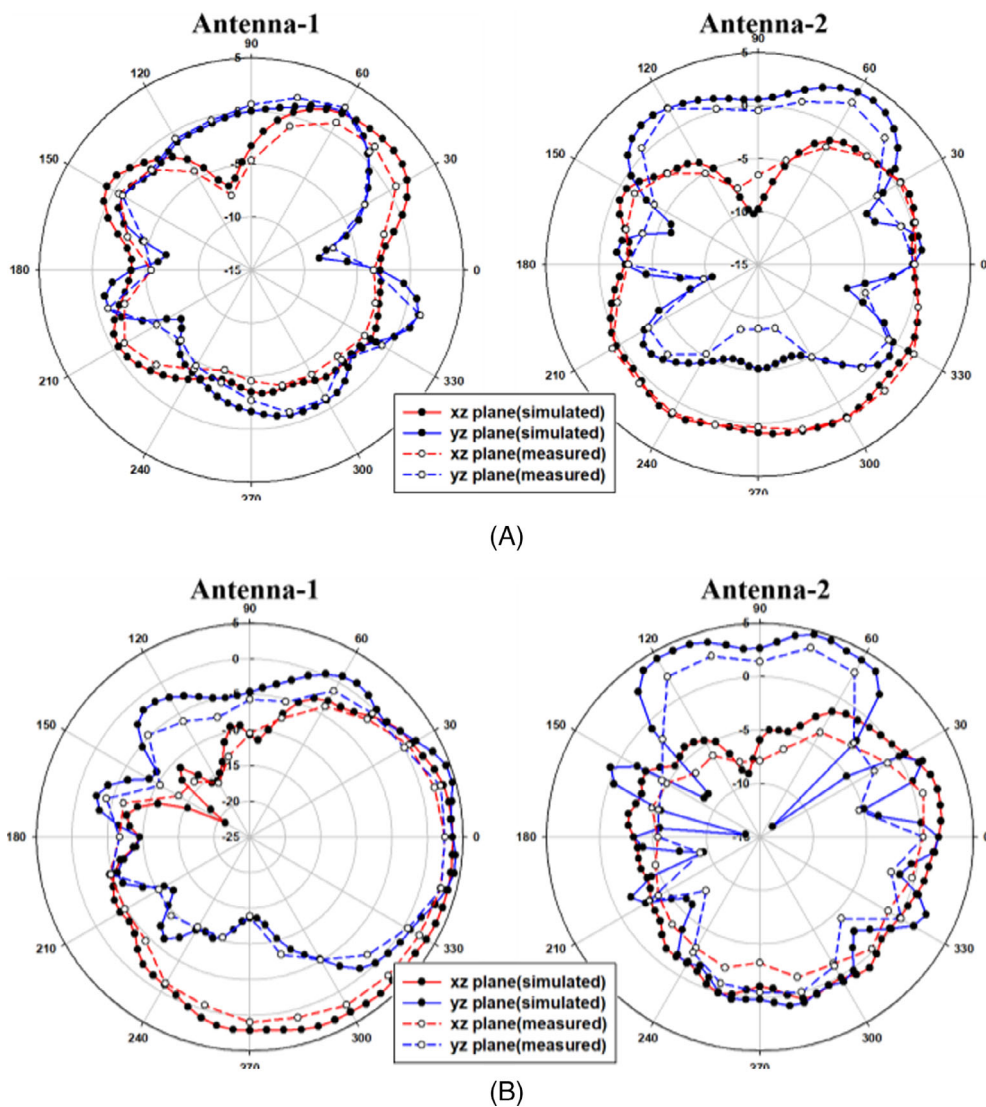


FIGURE 8 Simulated and measured radiation patterns: (A) at 3.5 GHz and (B) at 5 GHz

3.2 | Simulation and measurement

In this subsection, the fabrication was tested using a network analyzer and measured in a $6\text{ m} \times 3\text{ m} \times 3\text{ m}$ three-dimensional (3D) CTIA OTA anechoic chamber. The simulated and measured S -parameters of the proposed 8×8 MIMO antennas are given in Figure 6. As can be observed, the S_{11} and S_{22} curves fully cover the 3.5 GHz band and the 5 GHz band for 5G applications. It can be observed that the measurement data agree well with the simulation one only with a minor discrepancy, which may be attributed to the fabrication error, implementation accuracy, and the cable effect. Furthermore, it is seen that the isolation between any two antenna ports at the lower band and the higher band is over 18 and 16 dB, respectively, satisfying the engineering requirement in practical scenarios.

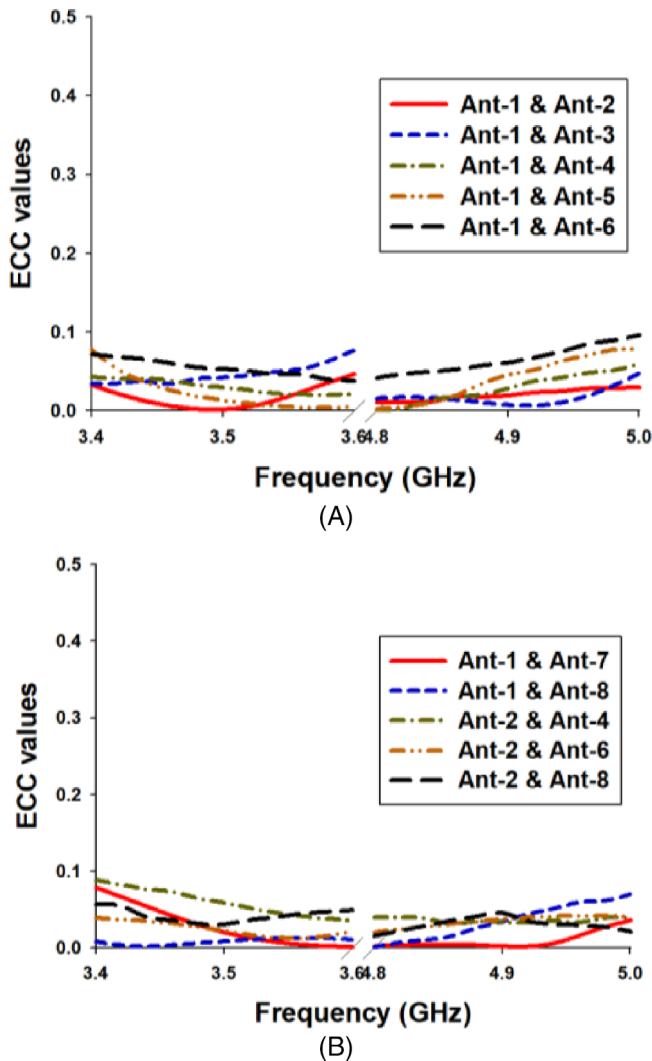


FIGURE 9 Measured ECC values of the fabricated 8×8 MIMO antenna array. ECC, envelope correlation coefficient; MIMO, multiple-input multiple-output

Additionally, the measured total radiation efficiencies are plotted in Figure 7, where it can be confirmed that both antennas can produce efficiencies over 60% in the dual operation bands. To verify the diversity performance of the proposed MIMO antenna module, the produced radiation patterns are displayed in the xz - and yz -planes, as shown in Figure 8. In both the lower band and higher band, it is seen that the maximum gains of Antenna-1 and Antenna-2 direct against each other, and their radiation patterns are approximately complementary, indicating the polarization diversity of the proposed MIMO antenna module.

3.3 | Diversity performance

Herein, correlation is an important figure of merit to measure the diversity performance of a MIMO antenna system. Accordingly, the envelope correlation coefficient (ECC) ρ_e is plotted in Figure 9, which is calculated from the vector properties (amplitude, phase, and polarization) of the complex 3D far-field radiation patterns.³³ It can be confirmed that the ECC values are all below 0.1, far lower than the acceptance criterion for mobile communications ($\rho_e < 0.5$).

Moreover, mean effective gain (MEG) is an important parameter to quantify the ability of the diversity antennas to receive electromagnetic power. The simulated MEGs of Antenna-1 and Antenna-2 are plotted in Figure 10. It can be seen that the MEG difference between the two antennas is less than 1 dB. For each antenna, the variation within the overall operation bands is also small (less than 1 dB). This property makes the proposed antennas a good MIMO antenna system with improved diversity

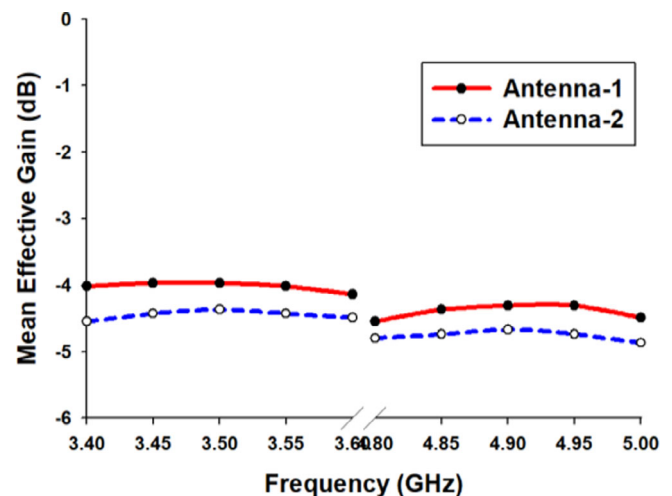


FIGURE 10 Calculated MEGs of the proposed MIMO antennas. MIMO, multiple-input multiple-output

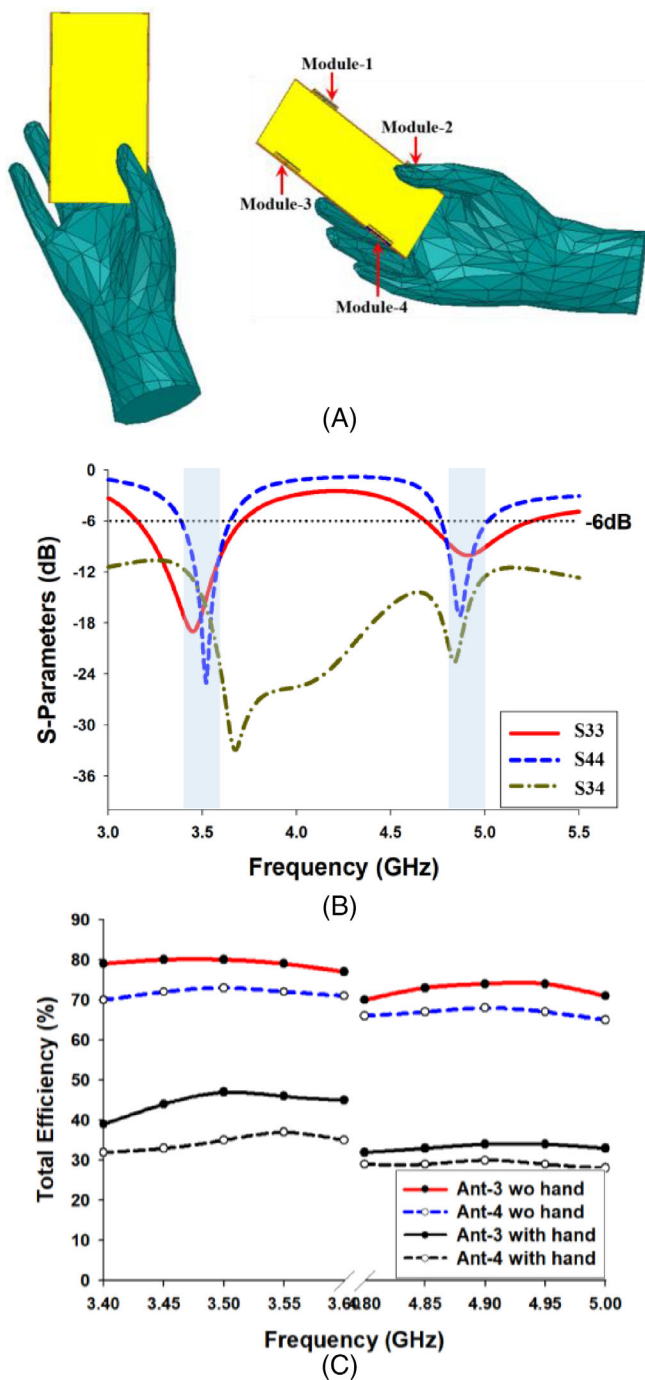


FIGURE 11 Hand effect in simulation: (A) simulation model, (B) S -parameters, and (C) simulated total efficiencies

performance. It is noted that the results of other antennas are omitted here for brevity because of the symmetry of the MIMO antenna array.

3.4 | Discussion on user's hand effect

The user's hand effect is further considered here to verify the feasibility of the proposed antennas in terminal

applications. Figure 11A presents the simulation model of the proposed MIMO antennas under the right-hand mode. Since Module-2 (Port 3 and Port 4) is closest to the human hand and has the severest degradation, the radiation performance of Module-2 only is investigated here for simplicity. As shown in Figure 11B, the S -parameters produced by Module-2 have a slight perturbation (when compared to Figure 7A) due to proximity to the human hand. Nevertheless, dual operation bands can still be covered, and the isolation between Port 3 and Port 4 is high enough. Furthermore, the simulated total efficiencies with and without the user's hand are plotted in Figure 10C. As can be observed, the total efficiencies decreased approximately by 3 dB due to the power absorption by the user's hand, which is comparable with those in References 14–16,19,21,25,29.

4 | CONCLUSION

A dual-band MIMO antenna module, consisting of a loop-type antenna and a dipole-type antenna, is proposed in this study. Each antenna element can achieve dual-band applications by effectively utilizing its dominant mode and higher mode resonances. The modal orthogonality at each operation band ensures the high isolation performance between the two antenna ports without adopting any complicated decoupling structures or matching networks. Furthermore, the structural compatibility allows the two antenna elements integrated into the front side and backside of a singular modular board. An 8×8 MIMO antenna array was simulated and measured. It is shown that the isolation between each two antenna element is higher than 16 dB, and the radiation efficiency of each antenna is over 65%. Moreover, the ECC values between each two antenna ports are below 0.1. In conclusion, the proposed technique has the advantages of high integration, multiband operation, high isolation, and low correlation, which can be a promising candidate for 5G MIMO applications.

DATA AVAILABILITY STATEMENT

Data sharing not applicable to this article as no datasets were generated or analysed during the current study.

ORCID

Longyue Qu  <https://orcid.org/0000-0001-5152-091X>

REFERENCES

- Boccardi F, Heath RW, Lozano A, Marzetta TL, Popovski P. Five disruptive technology directions for 5G. *IEEE Commun Mag.* 2014;52(2):74-80.
- Chaturvedi D, Kumar A, Raghavan S. Wideband HMSIW-based slotted antenna for wireless fidelity application. *IET Microw. Antennas Propag.* 2019;13(2):258-262.

3. Al-Wahhamy A, Al-Rizzo H, Buris NE. Efficient evaluation of massive MIMO channel capacity. *IEEE Syst J.* 2020;14(1):614-620.
4. Chang L, Yu Y, Wei K, Wang H. Orthogonally-polarized dual-antenna pair with high isolation and balanced high performance for 5G MIMO smartphone. *IEEE Trans. Antennas Propag.* 2020;68(5):3487-3495.
5. Piao H, Jin Y, Qu L. A compact and straightforward self-decoupled MIMO antenna system for 5G applications. *IEEE Access.* 2020;8:129236-129245.
6. Xu Z, Deng C. High-isolated MIMO antenna design based on pattern diversity for 5G mobile terminals. *IEEE Antennas Wirel Propag. Lett.* 2020;19(3):467-471.
7. Piao H, Jin Y, Qu L. Isolated ground-radiation antenna with inherent decoupling effect and its applications in 5G MIMO antenna array. *IEEE Access.* 2020;8:139892-139902.
8. Deng C, Liu D, Lv X. Tightly arranged four-element MIMO antennas for 5G mobile terminals. *IEEE Trans. Antennas Propag.* 2019;67(10):6353-6361.
9. Ren A, Liu Y, Yu H-W, Jia Y, Sim C-Y-D, Xu Y. A high-isolation building block using stable current nulls for 5G smartphone applications. *IEEE Access.* 2019;7:170419-170429.
10. Li Y, Sim C-Y-D, Luo Y, Yang G. High-isolation 3.5 GHz eight-antenna MIMO array using balanced open-slot antenna element for 5G smartphones. *IEEE Trans. Antennas Propag.* 2019;67(6):3820-3830.
11. Abdullah M, Kiani SH, Abdulrazak LF, et al. High-performance multiple-input multiple-output antenna system for 5G mobile terminals. *Electronics.* 2019;8(10):1-16. doi:10.3390/electronics8101090
12. Rosaline I, Kumar A, Upadhyay P, Murshed AH. Four element MIMO antenna systems with decoupling lines for high-speed 5G wireless data communication. *Int J Antennas Propag.* 2022;2022:1-13.
13. Sim C-Y-D, Liu H-Y, Huang C-J. Wideband MIMO antenna array design for future mobile devices operating in the 5G NR frequency bands n77/n78/n79 and LTE band 46. *IEEE Antennas Wirel Propag. Lett.* 2020;19(1):74-78.
14. Cai Q, Li Y, Zhang X, Shen W. Wideband MIMO antenna array covering 3.3-7.1 GHz for 5G metal-rimmed smartphone applications. *IEEE Access.* 2019;7:142070-142084.
15. Abdullah M, Kiani SH, Iqbal A. Eight element multiple-input multiple-output (MIMO) antenna for 5G mobile applications. *IEEE Access.* 2019;7:134488-134495.
16. Li Y, Sim C-Y-D, Luo Y, Yang G. Multiband 10-antenna array for sub-6 GHz MIMO applications in 5-G smartphones. *IEEE Access.* 2018;6:28041-28053.
17. Hei YQ, He JG, Li WT. Wideband decoupled 8-element MIMO antenna for 5G mobile terminal applications. *IEEE Antennas Wirel Propag. Lett.* 2021;20(8):1488-1452.
18. Deng C. Compact broadband multi-input multi-output antenna covering 3300 to 6000 MHz band for 5G mobile terminal applications. *Microw Opt Technol Lett.* 2020;62(10):3310-3316.
19. Hu W, Qian L, Gao S, et al. Dual-band eight-element MIMO array using multi-slot decoupling technique for 5G terminals. *IEEE Access.* 2019;7:153910-153920.
20. Cui L, Guo J, Liu Y, Sim C-Y-D. An 8-element dual-band MIMO antenna with decoupling stub for 5G smartphone applications. *IEEE Antennas Wireless Propag. Lett.* 2019;18(10):2095-2099.
21. Jiang W, Cui Y, Liu B, Hu W, Xi Y. A dual-band MIMO antenna with enhanced isolation for 5G smartphone applications. *IEEE Access.* 2019;7:112554-112563.
22. Yuan X-T, Chen Z, Gu T, Yuan T. A wideband PIFA-pair-based MIMO antenna for 5G smartphones. *IEEE Antennas Wireless Propag. Lett.* 2021;20(3):371-375.
23. Serghiou D, Khalily M, Singh V, Araghi A, Tafazolli R. Sub-6 GHz dual-band 8×8 MIMO antenna for 5G smartphones. *IEEE Antennas Wireless Propag. Lett.* 2020;19(9):1546-1550.
24. Wang M, Xu B, Li Y, Luo Y, Zou H, Yang G. Multiband multiple-input multiple-output antenna with high isolation for future 5G smartphone applications. *Int J RF Microw Comput Aided Eng.* 2019;29(7):e21758.
25. Guo J, Cui L, Li C, Sun B. Side-edge frame printed eight-port dual-band antenna array for 5G smartphone applications. *IEEE Trans. Antennas Propag.* 2018;66(12):7412-7417.
26. Su S-W, Lee C-T, Chen S-C. Very-low-profile, triband, two-antenna system for WLAN notebook computers. *IEEE Antennas Wirel Propag Lett.* 2018;17(9):1626-1629.
27. Chang L, Zhang G, Wang H. Dual-band antenna pair with lumped filters for 5G MIMO terminals. *IEEE Trans Antennas Propag.* 2021;69(9):5413-5423.
28. Sun L, Li Y, Zhang Z, Feng Z. Wideband 5G MIMO antenna with integrated orthogonal-mode dual-antenna pairs for metal-rimmed smartphones. *IEEE Trans. Antennas Propag.* 2020;68(4):2494-2503.
29. Ren Z, Zhao A. Dual-band MIMO antenna with compact self-decoupled antenna pairs for 5G mobile applications. *IEEE Access.* 2019;7:82288-82296.
30. Wong K-L, Lin B-W, Li W-Y. Dual-band dual inverted-F/loop antennas as a compact decoupled building block for forming eight 3.5/5.8-GHz MIMO antennas in the future smartphone. *Microw. Opt. Technol. Lett.* 2017;59:2715-2721.
31. Sun LB, Feng HG, Li Y, Zhang ZJ. Compact 5G MIMO mobile phone antennas with tightly arranged orthogonal-mode pairs. *IEEE Trans. Antennas Propag.* 2018;66(11):6364-6369.
32. Zheng M, Wang HY, Hao Y. Internal hexa-band folded monopole/dipole/loop antenna with four resonances for mobile device. *IEEE Trans. Antennas Propag.* 2012;60(6):2880-2885.
33. Vaughan RG, Andersen JB. Antenna diversity in mobile communications. *IEEE Trans. Veh. Technol.* 1987;36:149-172.

How to cite this article: Qu L, Piao H. Integrated dual-band multiple-input multiple-output antenna module using higher mode control for 5G applications. *Int J RF Microw Comput Aided Eng.* 2022;32(12):e23408. doi:10.1002/mmce.23408